Arch. Metall. Mater. **69** (2024), 3, 1005-1014

DOI: https://doi.org/10.24425/amm.2024.150921

H. WANG[1], N. ZHANG[1], M. WANG[1], F. YANG[2*]

EFFECT OF PARTICLE SIZE, LUBRICANT, AND HEAT TEMPERATURE ON THE FLOWABILITY OF Ni-BASED POWDERS FOR ADDITIVE MANUFACTURING

Gas-atomized Ni-based powder tends to agglomerate, directly impacting the spreadability of printing process. In this paper, three technical methods are applied to restore the powder flowability, including regulating particle size distribution, lubricant modification, and heating treatment. As particle size increases, powder regains flowability. However, the average particle size of GH3536 powders with flowability is greater than 46 μm, which cannot meet the demand for 3D printing (15-53 μm). The flowability of GH3536 powder can be restored by adding zinc stearate lubricant. After lubricant modification, the printed samples display a 16% increase in elongation, along with a little improvement in tensile strength. This paper also investigates the flow properties change of raw powder heated at 100°C, 200°C, 300°C, and 400°C. When the temperature rises beyond 400°C, powder flowability fully returns, along with oxygen content increasing. Overall, the lubricant modification technique is appropriate in actual manufacturing, but the flow rate value of powders is typically high, exceeding 70 s/50 g. Increasing particle size and heat treatment can improve powder flowability and the flow rate of powder is less than 20 s/50 g.

Keywords: Ni-based powder; flowability; particle size distribution; lubricant modification; heating treatment

1. Introduction

Nowadays, a growing number of manufacturers are turning to additive manufacturing (AM) for complex-shaped component fabrication in oil and gas, aerospace, energy, and defense industries. Laser powder bed fusion (LPBF) is one of the most widely used AM technologies and has been extensively applied in steam turbines, aero engines, offshore subsea, and tool manufacturing [1]. Moreover, LPBF permits near-net forming, which lowers processing costs and is appropriate for small production runs [2]. In the printing process, the quality of gas atomized raw powder has a significant impact on the performance of final component. In order to produce excellent parts, raw powder must have good flowability, small particle size, narrow particle size distribution, high sphericity and packing density [3-6]. However, in the gas atomization process, powder particles often adhere and agglomerate together, resulting in the reduction of powder flowability. The flow behavior of raw powders has long been a question of great interest in AM field. Gravity and interparticle adhesion have the most effects on powder flowability. High cohesion between powder particles, mainly attributed to the tiny force more potent than self-gravity, causes the powder to clump together [7,8]. Additionally, particle shape [9,10] and size distribution [11,12] play a significant role in powder flowability. Reduced flowability and filling efficiency result from increased cohesiveness and decreased self-gravity caused by smaller particles [13]. Since the individual mass of particles is greater, and their gravity is likewise greater, powders with big particle size or high-density typically demonstrate superior flowability. As the amount of satellite powder and shaped powder increases, the friction between particles makes it challenging for powders to flow. Besides, other variables such as temperature [14], water content [15,16], and electrostatic voltage [17], also affect powder flowability.

To achieve the uniform distribution of powder feedstock throughout the build area, good powder flow is essential for LPBF process. Highly cohesive powders are challenging to spread and produce inhomogeneous patches that alter their stacking density, thermal conductivity, and optical characteristics [18,19]. Therefore, the mass production of gas-atomized powders, except for Ti powder and the continuous expansion of metal additive technology significantly depend on achieving the declustering and dispersion of agglomerate powders and increasing powder flowability.

[1] CHINA MACHINERY INSTITUTE OF ADVANCED MATERIALS (ZHENGZHOU) CO., LTD, ZHENGZHOU 450001, CHINA
[2] UNIVERSITY OF SCIENCE AND TECHNOLOGY BEIJING, INSTITUTE FOR ADVANCED MATERIALS AND TECHNOLOGY, BEIJING 100083, CHINA & UNIVERSITY OF SCIENCE AND TECHNOLOGY BEIJING, SHUNDE INNOVATION SCHOOL, GUANGZHOU 528399, CHINA

* Corresponding authors: hjsososo54@gmail.com

Over the past few years, researchers and industry participants have boosted their efforts to enhance powder performance to avoid defects in printing metal parts. Traditional methods include adjusting equipment and processes at the gas atomization stage, such as expanding the atomization chamber capacity [20,21], using new and efficient atomization nozzles [22-24] increasing melt overheating, and controlling gas atomized pressure and liquid flow rate [25]. However, the gas-atomized method of producing metal powders is highly unstable and restricted to single-batch qualities. Numerous experimental processes and equipment upgrades raise production costs without producing references that can be relied repeatedly. Post-treatment of the aerosolized powder is another method for flow enhancement, where the flowability improvement is pursued by a focused examination of various factors impacting powder flow. In order to improve the flowability of fine metal powder as well as to reduce their agglomeration, various approaches have been developed, including surface modification [26] and dry coating technique [27].

In this study, we focused on gas-atomized Ni-based superalloys powder with poor flowability. Three methods, including adjusting particle size distribution, microfine lubricant modification, and heat treatment, were used to improve the flow properties of gas-atomized Ni-based powder. Additionally, various techniques were employed to gauge powder flowability changes.

2. Experimental proceduce

2.1. Raw powders and characterization

The raw powder used in the study was gas-atomized GH3536 powder (providing from Jiangsu Vilory Advanced Materials Technology Co., China) with D10 = 18.29 μm, D50 = 31.64 μm, and D90 = 53.20 μm. Figs. 1(a, b) show GH3536 powder morphology, and there is almost no internal pore observed. Micron-scale zinc stearate powder was also used as a lubricant additive to regulate powder flowability (providing from Hebei Baiyilian Chemical Technology Co., China), which would be discussed later. Zinc stearate is a common lubricant for powder metallurgy, which has an elemental content of Zn of 13-14.5% and a melting point of about 120°C. Zinc stearate powder is in the form of irregular lumps with an average particle size of <45 μm. During the sintering process of powder metallurgy, when the temperature exceeds 250°C, zinc stearate will decompose to produce zinc, zinc oxides, and other compounds. Zinc stearate has been frequently used in powder metallurgy [28,29], but it has fewer application cases in additive manufacturing. Consequently, this study selects zinc stearate as a lubricant to investigate the influence on the flowability of GH3536 powder and the performance of printed components.

Powder morphology was observed using scanning electron microscopy (SEM, Supra55). All powders were dried at 80°C for 8 h and then cooled to room temperature before being used. The relative number of various sized particles was used to determine particle size distribution using a BT-3000 laser particle sizer.

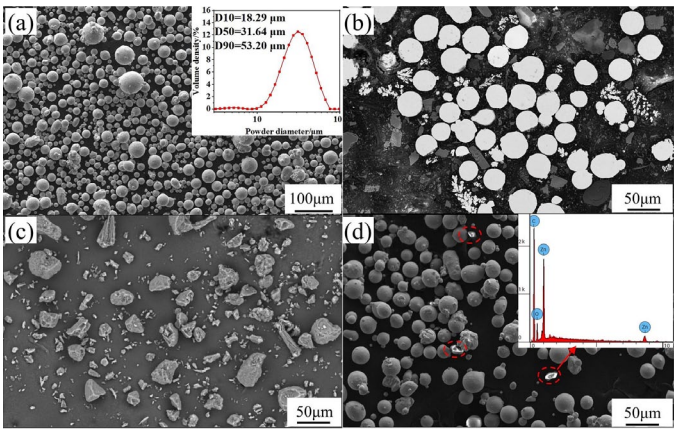

Fig. 1. SEM image of (a) GH3536 powder, (b) GH3536 powder section, (c) zinc stearate powder, and (d) mixture of GH3536 powder with zinc stearate

These factors of mean size, distribution width, and distribution mode affect the powder flowability. The following equation describes the span, an additional parameter that indicates the width of size distribution:

$$Span = \frac{D_{90} - D_{10}}{D_{50}} \quad (1)$$

where D10, D50, and D90 denote the point where the cumulative particle size distribution is 10%, 50% and 90%, respectively. Sphericity was used to gauge the regularity of metal powders [30]. A Zeiss optical microscope (OM) was used to observe the powder's sphericity, and data were collected using ProImaging. We examined powder morphology to determine whether the powder sphericity was close to 1.

2.2. Powder reprocessing

In this study, raw GH3536 powders didn't pass through Hall funnel, which were used to investigate the causes for weak flowability. Accordingly, three post-treatments were carried out to improve the flowability, including adjustment of particle size distribution, modification with lubricants, and heat treatment.

2.2.1. Powder sieving and mixing

Powders were sieved into various groups using standard mesh. Then, powder particles were heated in a vacuum furnace at 105°C for 2 h. After that, powders were transported to a screening machine to sieve under vibration for 10 min. The captured powders with different particle sizes were displayed in Fig. 2. It was evident that the smaller the particle size, the more prominent the agglomeration phenomenon was. Finally, different-sized powders were combined to achieve a wider particle size distribution than original powder. The mixing principle was to increase coarse powder and decrease fine powder gradually. Particle size was measured using D50 values for comparison. The fluidity of

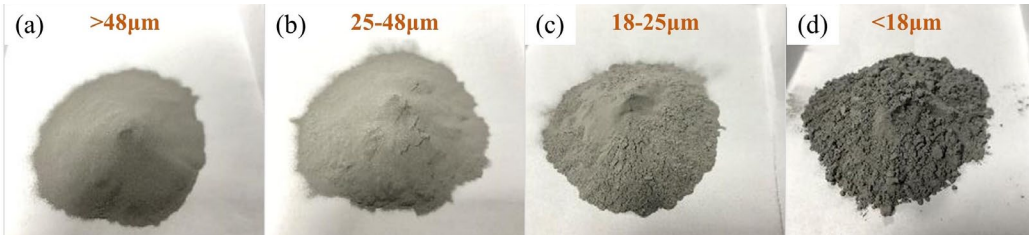

Fig. 2. Powder batches with different sizes: (a) >48 μm, (b) 25-48 μm, (c) 18-25 μm, and (d) <18 μm

TABLE 1

Particle size distribution and flow rate of mixed powders

	>48 μm	25-48 μm	18-25 μm	<18 μm	D10 (μm)	D50 (μm)	D90 (μm)	Mean size (μm)	Span	Flow rate (s/50g)
Powder 1	15.00%	55.00%	20.00%	10.00%	18.29	31.64	53.2	34.38	1.10	—
Powder 2	17.50%	57.50%	17.50%	7.50%	18.97	32.76	53.96	35.23	1.07	—
Powder 3	20.00%	60.00%	15.00%	5.00%	20.62	34.27	53.48	36.12	0.96	—
Powder 4	22.50%	62.50%	12.50%	2.50%	23.96	36.36	54.36	38.23	0.84	—
Powder 5	30.00%	60.00%	10.00%	0	22.56	38.90	62.58	41.35	1.03	—
Powder 6	32.50%	62.50%	5.00%	0	26.98	40.69	61.39	43.02	0.85	—
Powder 7	37.50%	60.00%	2.50%	0	27.35	42.81	66.26	45.47	0.91	—
Powder 8	45.00%	55.00%	0	0	27.29	43.97	71.84	47.70	1.01	18.77±0.09
Powder 9	50.00%	50.00%	0	0	29.9	47.79	73.25	50.31	0.91	16.43±0.03
Powder 10	55.00%	45.00%	0	0	34.02	51.09	77.16	54.09	0.84	12.18±0.04

these powders was tested using Hall flowmeter. Ten batches of powders with various particle size distributions were produced after mixing, as shown in TABLE 1. These powder batches were used in the following modification experiment.

2.2.2. Powder modification

GH3536 powders and zinc stearate powders were processed using the following steps. First, 0.05 wt.% zinc stearate lubricant powder was added separately to the ten batches of powders in Section 2.2.1. Second, the mixture was done in a single cone blender, rotating at 10 RPM for 30 min. Then, powder flowability changes were detected. After mixing, zinc stearate particles were attached on GH3536 particle surface, as shown in Fig. 1(d).

2.2.3. Powder heat treatment

GH3536 powders were respectively heated at 100°C, 200°C, 300°C, and 400°C under high-purity argon gas. The heating time was set to 2 h, with a heating rate of 10°C/min, and air cooling was applied. Oxygen and nitrogen contents were evaluated using ELTRA ONH-2000 analyzer.

2.3. Powder measurement

Spreadability, a significant issue impacting the quality of powder bed fusion (PBF), is closely related to powder flow properties. In general, the smoother the powder flows, the more homogeneous the powder spreads, and the less defect there is in the printing process. In this study, we attempted to assess the powder spreadability using a fineness meter (Labman Automation Ltd., China), as shown in Fig. 3. This method consisted of putting a small quantity of powder in a groove with a depth varying from 100 μm to 0 μm and spreading the powder with a blade along the groove. OM machine was used to observe the powder surface on the gauge. Then, powder samples in three areas of 80 μm, 50 μm, and 10 μm on the gauge were glued with conductive tape, respectively. The distribution of powders was observed using electron microscope. The spreadability can be qualitatively assessed by comparing the quality and the formation of defects in the powder layer.

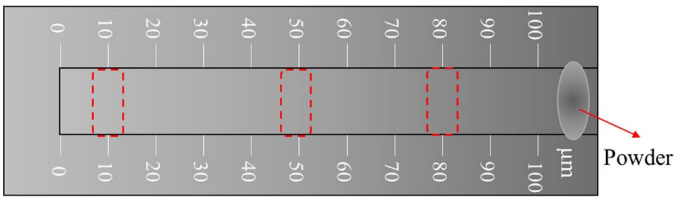

Fig. 3. A schematic of the fineness gauge (0-100) μm with the locations (red squares) where the samples were taken

2.4. 3D printing verification

3D printing verification of GH3536 powder and modified GH3536 powder with 0.05 wt.% zinc stearate was conducted to determine the impact of increased powder flowability on the printing quality. Printing experiments were performed using a LiM-X650H LPBF machine (Tianjin Lim Laser Technol-

ogy Co., Ltd, China) equipped with a single-mode ytterbium fiber laser with a spot size of ~70 μm and a maximum power of 500 W. To produce samples with lowest porosity and highest density, the optimal processing parameters were selected as below:

- Laser power: 100 W for first scan, 400 W for second scan.
- Scanning speed: first scan 75 mm/s, second scan 500 mm/s.
- Layer thickness: 30 μm.
- Hatch distance: 160 μm.

Blocks with dimensions of $10 \times 80 \times 10$ mm^3 were produced for microstructural characterization and tensile tests. Each sample was produced in 0° orientation to the basal X-Z plane, according to a scheme presented in Fig. 4(a). Parts of the printed samples were performed heat treatment at 1177°C for 1 h followed by Ar gas cooling, while the others remained initial state. Tensile test samples shown in Fig. 4b were cut out from the produced blocks by means of Electro Discharge Machining (EDM). Tensile testing equipment (UH4304GL, China) was used to test the tensile properties at room temperature with a crosshead travel speed of 1 mm/min. Microstructure was observed in longitudinal sections of final tensile samples. To observe microstructure, printed samples were etched using Kalling's solution, consisting of 0.5 g $CuCl_2$, 10 ml HCl and 40-80 ml ethanol.

3. Result and discussion

3.1. Powder size distribution

Powder size distributions of the ten batches of mixed powder are shown in Fig. 5. Powder particle sizes of D10, D50, and D90 and the corresponding flow rate values are listed in TABLE 1. It can be seen from Fig. 5 that the particle size distribution from Powder 1 to Powder 10 is gradually shifted to the right, and the powder mean size gradually increases. With the increase of particle size, the flowability increases. In the case of increasing coarse particles, the self-gravity of powder particles gradually surpasses the microscopic interaction forces between powder particles. However, even for the powder that initially shows flowability (Powder 4), the average grain size is still as high as 43.97 μm. The particle size of powders with flowability has deviated from the appropriate range of 15-53 μm for LPBF.

3.2. Lubricant effect

Fig. 6 compares the flow rates of the ten powders with 0.05 wt.% lubricant addition. It can be seen that the raw powders still do not show flowability. With lubricant addition, all the powders regained flowability. With the increase of powder size, powder flowability increases. The variation of powder flow behavior can be seen in the powder-free flow bundle in Fig. 6. Raw powder could not pass the funnel hole. After modification, powders can flow easily, and as particle size increases, the powder beam stream seems more continuous and denser. The reason is mainly related to a decrease of van der Waals forces (Fvdw) due to nano lubricant particle addition. According to the mechanism proposed by Rumpf [31], the increase in flowability results from reduced roughness on the particle surface. Lubricant acts as spacer, and thus reduces the Fvdw between powder particles.

Additionally, the powder modified with 0.05 wt.% zinc stearate is used for printing, and the printing of raw powder is also carried out for comparison. It can be seen from Table

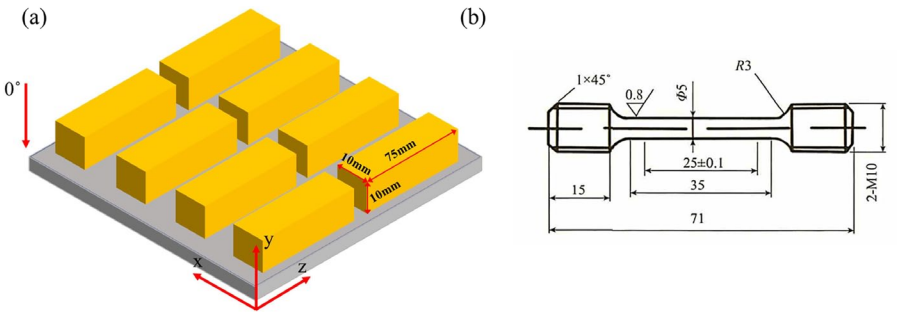

Fig. 4. (a) Scheme of samples printing orientation and (b) tensile test samples

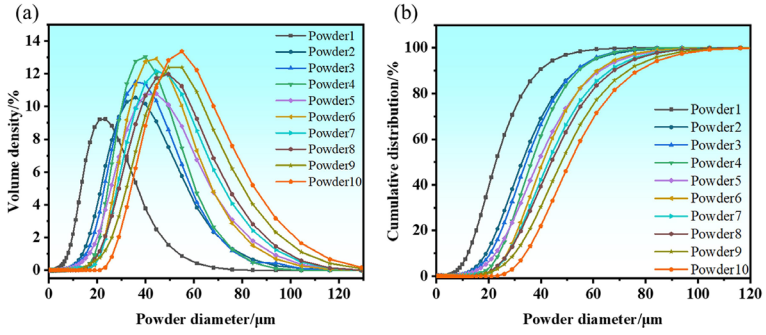

Fig. 5. Distribution of (a) powder volume density, and (b) cumulative distribution density

3 that modified powder regains flowability, and the measured value of flow rate is much higher than traditional gas-atomized Ni-based superalloy powder (≤18 s/50 g) [32]. In addition, the bulk density of modified powder increases from 4.16 g/cm^3 to 5.17 g/cm^3. Considering that the powder is in a free-stacking state in the actual printing process, the increase of bulk density is very important.

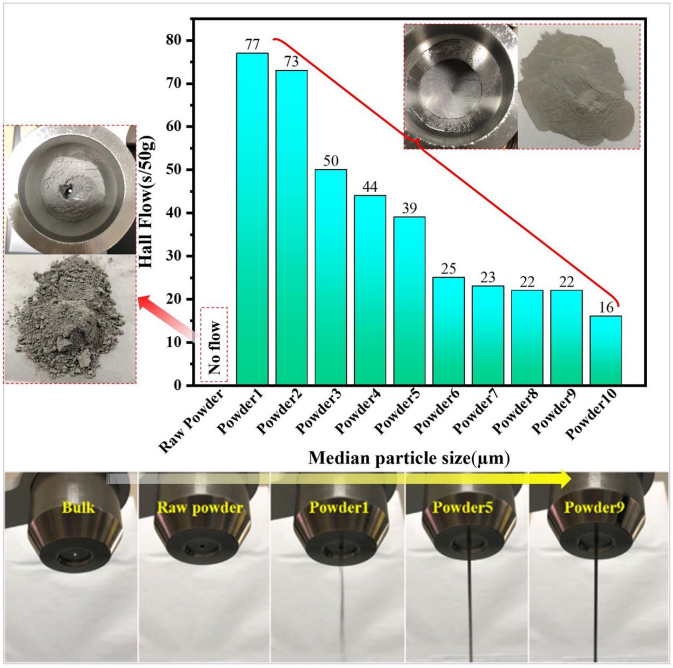

Fig. 6. Hall flow rate variation of different powders with lubricant modification

Fig. 7 shows the melt pool and microstructure of printed GH3536 samples after chemical etching. Although GH3536 powders are modified using lubricant, the fusion boundary morphology and microstructure of printed sample are similar to that of GH3536 sample without powder modification, as shown in Figs. 7(a-b). However, many tiny pores are found in Fig. 7(a). After heat treatment, the microstructure of printed GH3536 superalloys changes significantly. Carbide networks with clearly visible

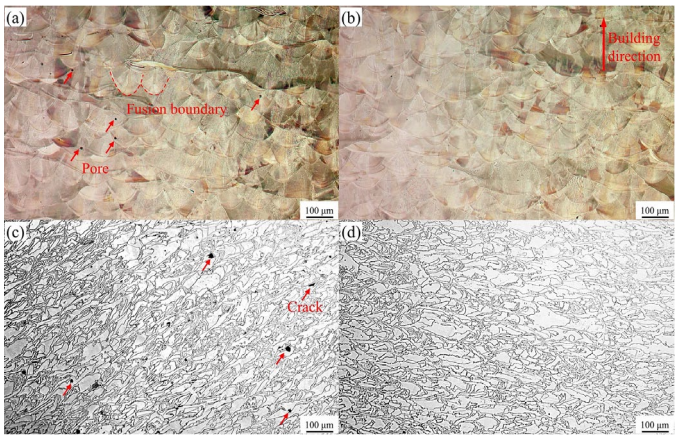

Fig. 7. OM images of printed GH3536 samples (a) as-printed, raw (b) as-printed, modified (c) heat-treated, raw (d) heat-treated, modified

boundaries are found in samples after heat treatment. As shown in Fig. 7(c), microcracks are found in the printed GH3536 sample using raw powders. In contrast, no micro-cracks are detected in the GH3536 sample using modified powders (Fig. 7(d)). These results further confirm that the higher the packing density of powder, the less cracks are formed in the LPBF process.

Fig. 8 shows elemental distribution of pure GH3536 and modified samples. It can be found that there is no significant difference in the elemental distribution between pure GH3536 and modified samples (Fig. 8a, c). Zn elements and zinc oxides were not found in the modified GH3536 sample by EDS (Fig. 8c). After heat treatment, the Cr and Mo elements were enriched around the grain boundaries both in the pure GH3536 and modified samples, which is typical of carbide feature [33]. This finding indicates the addition of zinc stearate has no discernible impact on the microstructure and phase evolution of GH3536 samples after heat treatment. It also confirms that the added zinc stearate particles are evaporated during the printing process, implying that the lubricant does not instigate defect.

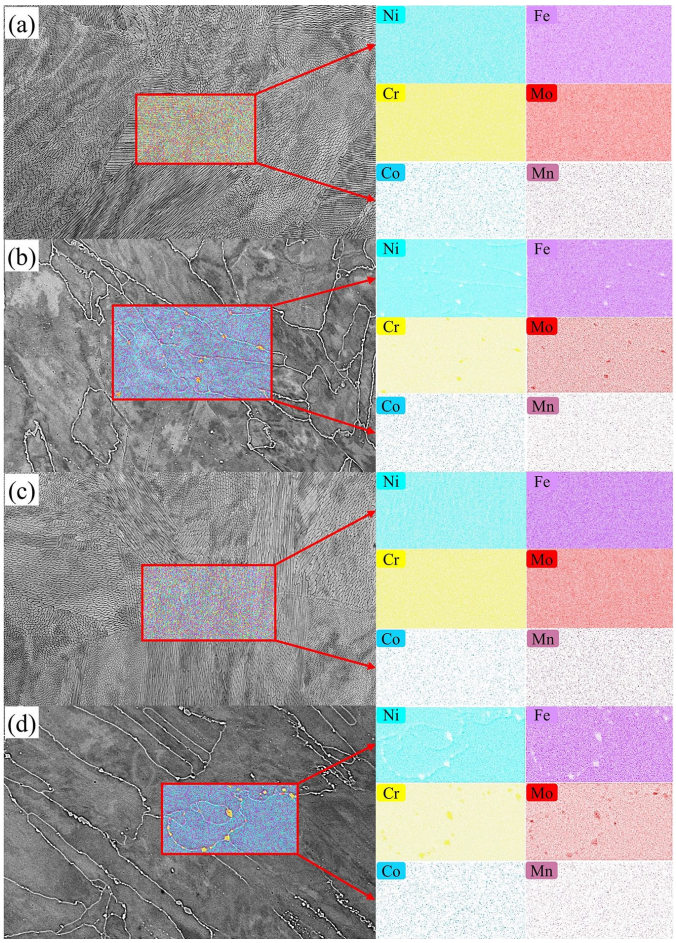

Fig. 8. Elemental mapping analysis of LPBF GH3536 sample. (a) as-printed, raw (b) as-printed, modified (c) heat-treated, raw (d) heat-treated, modified

Fig. 9 and TABLE 2 show the stress-strain results of printed GH3536 superalloys. After modification, the yield strength (YS) of printed GH3536 sample increases from 714.48 MPa to

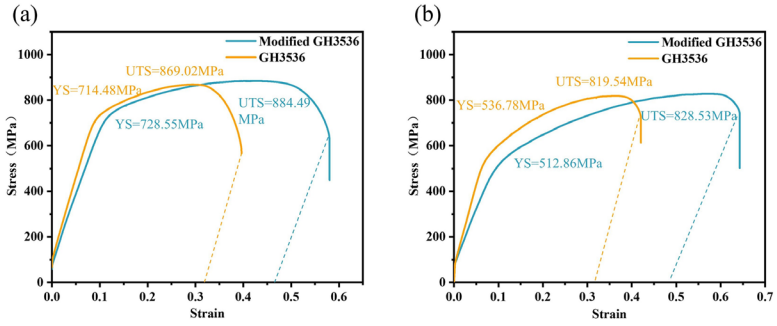

Fig. 9. Stress-strain curves of LPBF-processed GH3536 superalloys (a) without heat treatment, and (b) with heat treatment

TABLE 2

Physical properties of raw powder and modified powder

	Bulk density	Flow rate (s/50 g)	Relative density (%)	Printed samples			Printed samples with heat treatment		
				UTS (MPa)	YS (MPa)	EL. (%)	UTS (MPa)	YS (MPa)	EL. (%)
Raw powder	4.16	—	99.8	869.02	714.48	31.74	819.54	536.78	32.81
Modified powder	5.17	74-77	99.9	884.49	728.55	47.45	828.53	512.86	48.31

728.55 MPa, while the ultimate tensile strength (UTS) increases from 869.02 MPa to 884.49 MPa. Meanwhile, the elongation (EL.) increases from 31.74% to 47.45%. After heat treatment, UTS, YS and EL, show a decreasing trend. It is worth noting that YS has a distinct decrease, from 728.55 MPa to 512.86 MPa. From Fig. 9, it is clear that the ductility of LPBF-processed GH3536 sample is significantly improved with the addition of zinc stearate lubricant.

Fig. 10 shows the fracture morphology of two types of tensile samples before and after heat treatment, which confirms the improvement of the mechanical properties of the modified GH3536 material. As shown in Fig. 10a and c, defects were more pronounced on the fracture surface of the unmodified GH3536 samples. The surface of the unmodified GH3536 fracture shows obvious cracks (about 100 μm in length), as shown in Fig. 10a. There were many deep poles on the fracture surface of the unmodified GH3536 after heat treatment, and the size of the poles was different. These internal defects acted as stress concentrations and facilitated fracture failure. Only a few small pores were found on the fracture surface of the modified specimen and no obvious cracks were found, as shown in Fig. 10c. Many small dimples were detected on the fracture surface of the modified sample after heat treatment, and there was less porosity. This finding is consistent with previous experimental data and indicates a significant improvement in the ductility of modified samples. Therefore, the presence of fewer internal defects in the modified material samples was important for mechanical properties improvement compared with the unmodified GH3536.

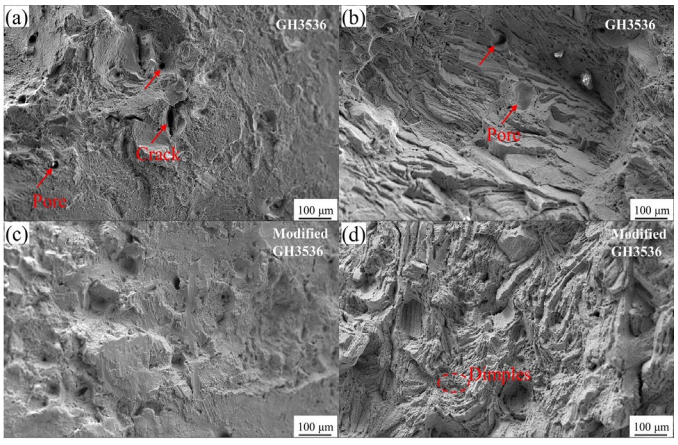

Fig. 10. Tensile fracture morphology of as-fabricated samples (a) as-printed, raw (b) as-printed, modified (c) heat-treated, raw (d) heat-treated, modified

Better powder flowability provided by lubricant is the key to preventing powder agglomeration. The lubrication mechanism of zinc stearate is shown in Fig. 11. Particle-particle contact creates cohesive forces (mainly van der Waals force). The fine particle shows cohesion greater than its own gravity, i.e. $F_0 > G$, which leads to powder aggregation and poor flowability. Hammaker [34] gives the formula for the F_{vdw} force between the two particles:

$$F_{vdw} = \frac{A}{12Z_0^2}\frac{D_1 D_2}{D_1 + D_2} \tag{2}$$

Where A is the Hammaker criterion. D_1, D_2 is the diameter of the contact particle. Z_0 is the distance between particles, usually taken as 4 Å. When lubricant is added to the powder and fully mixed, a large number of broken lubricant particles are adsorbed on the surface of the original particles, forming a thin film. Thus, there is particle-additive-particle-contact resulting in a higher distance of Z_0 between the powder particles. According to Formula (2), increasing Z_0 results in a significant decrease in F_{vdw}, i.e. $F_1 < F_0$. The gravitational G of the particles did not change and played a more dominant role, increasing the flowability of the powder. The addition of lubricant reduces the friction

between powder particles, making it easier for small particles to fill the gaps between large particles. Large voids in poorly flowing powder were not effectively filled compared to well-flowing powder, which could contribute to larger defects in parts processed by laser powder bed fusion (LPBF). The enlarged pore size may act as a crack initiator under tensile loading and lead to poor mechanical properties of LPBF parts. In addition, more researches are required to identify whether the elements in the lubricant are responsible for the increasing mechanical properties. However, considering its high volatility of zinc stearate at the high temperature of laser melting and the small amount of addition, this study concludes that the performance improvement of printed part is not much related to the chemical composition of lubricant itself [36].

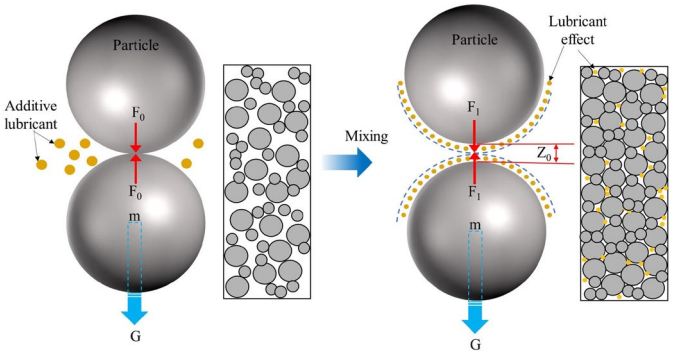

Fig. 11. Lubrication mechanism of zinc stearate in GH3536 powder

3.3. Powder heat treatment

TABLE 3 lists the flowability of raw powder and processed powders. Each powder is analyzed three times with negligible variation. The flowability of raw powders and powders heated at 100-200°C cannot be measured by Hall flow rate due to their high cohesion energy [37,38]. The powder begins to regain flowability after heating at 300°C, but the fluidity is lower than powder heated at 400°C.

TABLE 3

Flowability of raw powder and processed powders

Processing temperature	Flowability (s/50 g)
Raw powder	—
100°C	—
200°C	—
300°C	25-28 (Passable)
400°C	13-14 (Fair)
Reference [30]	≤18

Powder packing and corresponding repose angles of the four heated powders after Hall flow test are shown in Fig. 12. The response angle of powder heated at 100°C is relatively high at about 43°. The stacking hill of powders heated at 200°C, 300°C and 400°C shows relative smooth slope, and the corresponding response angles decrease to 39°, 34° and 27°, which is corresponding to the flowability evolution [39]. After heat treatment, the powder appearance develops with temperature increasing. As indicated in Fig. 12a, powders heated at 100°C demonstrate an ashy color similar to raw powder, while its spreadability is inferior compared to other powders heated at higher temperatures (Figs. 12c,d). The optical color gradually changes to brown when heated at 400°C as shown in Fig. 12d. According to Liu et al. [40], a fluidization effect is achieved when the powder is heated in a flowing argon environment. High-temperature fluidization has the potential to modify the powder and increase powder flowability. This is due to the collision between high-temperature gas molecules and powders, which produces kinetic energy exchange and increases the collision energy of powder particles. The collision and shear between particles make irregular powder bump and angles become ground, and thus the sphericity is improved to some extent [41].

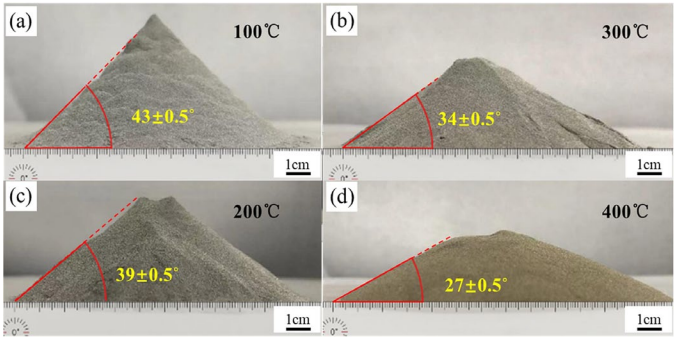

Fig. 12. Repose angles of GH3536 powders heated: (a) 100°C, (b) 200°C, (c) 300°C, and (d) 400°C

The effect of heat treatment temperature on spreadability was assessed using a fineness meter (100 μm). The results show that heating temperature significantly affect the scalability, as shown in Fig. 13. For powders heated at 100°C and 200°C, the powder cannot be spread and is almost invisible at all particle sizes. This means that powders agglomerate and are completely scraped away by the blade. For powders heated at 300°C, the powder becomes more spreadable. However, when the gauge depth changes from 80 μm to 50 μm, and to 10 μm, powder aggregation is observed. The powder spreads best when heated at 400°C. At measuring depths of 80 μm and 50 μm, the powder layer spreads uniform and no significant defects are observed. Beyond 10 μm limit, some particles are scraped by the blade, leaving some small particles observed. Although it is not perfect, the method is simple and provides an indication of the flow behavior of printing powder.

Fig. 14 summarizes the apparent density and tap density of the four powders. It can be seen that the variation of apparent density and tap density follows the rule of flowability. As the heating temperature increases, the apparent density increases. In this study, the highest apparent density (4.52 g/cm^3) is obtained after heating at 400°C, and the highest tap density (5.32 g/cm^3) is obtained in the powder heated at 200°C. The results indicate that the heating treatment can significantly weaken the bridg-

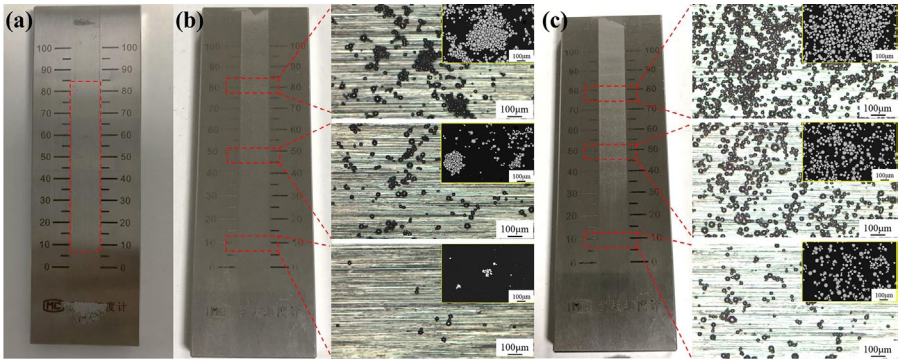

Fig. 13. Effect of heating temperature on spreadability of GH3536 gas atomized powder measured using a fineness meter: (a) 100-200°C, (b) 300°C, and (c) 400°C

ing effect between particles and increase the packing density of powders. Besides, the tap density shows no big difference, indicating that vibration can counteract the mutual repulsion of powder particles.

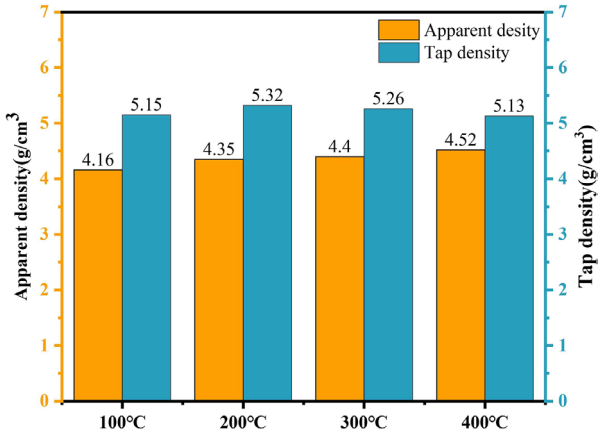

Fig. 14. Apparent density and tap density of processed powders

Fig. 15 compares the impurities content of raw powder and processed powders. It can be found that the oxygen and nitrogen contents increase with increasing heating temperature. The oxygen content of powders heated at 400°C is relatively high (478 ppm), which reveals that high temperature can introduce

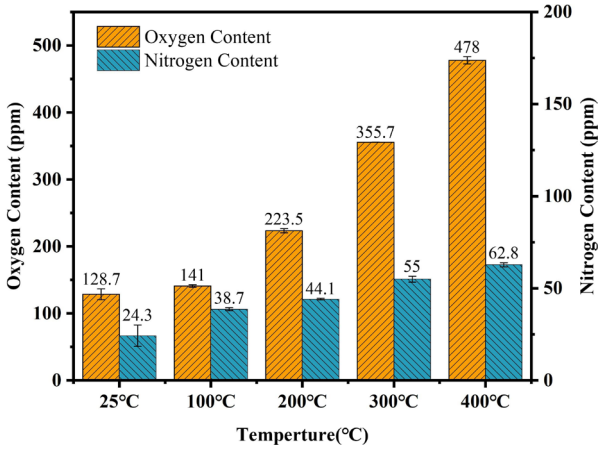

Fig. 15. Impurities content of raw powder and processed powders

the oxidization on particle surface. Marcu et al. [42] conclude that the oxide film formed on powder surface can improve the powder roughness, reduce the friction between particles, and increase the flowability. Observing powder surface state, clear surface patterns can be observed with no significant differences, as shown in Fig. 16. Further sectional observation shows that the heat treatment temperature has no obvious effect on the internal microstructure evolution of the powder, because the experimental temperature is lower than the phase transition temperature of the powder. Ding et al. [43] observe that the increase in oxide layer thickness of Ti powder heated at 600°C for 10 min is only about 10 nm. Therefore, it is difficult to observe significant changes of powder surface under electron microscope view.

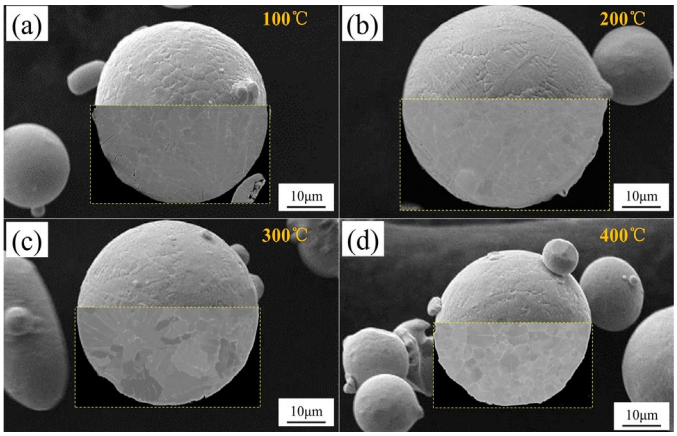

Fig. 16. Powder surface morphology and cross-section microstructure of GH3536 powders heated at (a) 100°C, (a) 200°C, (c) 300°C, and (d) 400°C

4. Conclusion

In this study, three technical methods of adjusting powder particle size, lubricant modification, and heat treatment are used to restore the flowability of gas atomized GH3536 powder. The following conclusions can be obtained.

(1) By adjusting the particle size distribution of GH3536 powder, the powder shows flowability when D10 > 27.29 μm, D50 > 43.97 μm, D90 > 71.84μm. Its own gravity gradually

outweighs the micro force between particles. However, the increased particle size of adjusted powder cannot meet the demand for conventional 3D printing.

(2) With lubricant addition, powder flowability is restored. The apparent density of modified powder increases to 5.03 g/cm^3. Besides, UTS and EL. of printed samples using modified powders increase by 15.4 MPa and 15.71%. Lubricant addition reduces the friction between particles and increases powder packing density, and thus improves mechanical performance.

(3) The repose angle, spreadability, packing density, and impurity content of powders increase with the increasing heating temperature. The powder heated at 400°C regains persistent flowability. Heating at high temperature magnifies powder surface oxidation, which decreases inter-powder interaction force and improves flowability.

Acknowledgment

This study was funded by the Key Project of the Defense Industrial Technology Development Program (Grant No. JCKY2022×××B207).

REFERENCES

[1] S. Irukuvarghula, H. Hassanin, C. Cayron, M. Aristizabal, M. Attallah, M. Preuss, Effect of Powder Characteristics and Oxygen Content on Modifications to the Microstructural Topology during Hot Isostatic Pressing of An Austenitic Steel. Acta Mater. **172** (15), 6-17(2019). DOI: https://doi.org/10.1016/j.actamat.2019.03.038

[2] D. Gu, X. Shi, R. Poprawe, D.L. Bourell, R. Setchi, J. Zhu, Material-Structure-Performance Integrated Laser-Metal Additive Manufacturing. Science **372** eabg1487 (2021). DOI: https://doi.org/10.1126/science.abg1487

[3] D.D. Gu, W. Meiners, K. Wissenbach, R. Poprawe, Laser Additive Manufacturing of Metallic Components: Materials, Processes and Mechanisms. Int. Mater. Rev. **57**, 133-164 (2012). DOI: https://doi.org/10.1179/1743280411Y.0000000014

[4] M. Vaezi, H. Seitz, S. Yang, A Review on 3D Micro-Additive Manufacturing Technologies. Int. J. Adv. Manuf. Technol. **67**, 1721-1754(2013). DOI: https://doi.org/10.1007/s00170-012-4605-2

[5] J.A. Muñiz-Lerma, A. Nommeots-Nomm, K.E. Waters, M. Brochu, A Comprehensive Approach to Powder Feedstock Characterization for Powder Bed Fusion Additive Manufacturing: A Case Study on AlSi7Mg. Materials **11** (12) 2386 (2018). DOI: https://doi.org/10.3390/ma11122386

[6] A.B. Spierings, M. Voegtlin, T. Bauer, K. Wegener, Powder Flowability Characterisation Methodology for Powder-Bed-Based Metal Additive Manufacturing. Prog. Addit. Manuf. **1**, 9-20 (2016). DOI: https://doi.org/10.1007/s40964-015-0001-4

[7] M. Krantz, H. Zhang, J. Zhu, Characterization of Powder Flow: Static and Dynamic Testing. Powder Technol. **194** (13), 239-245 (2009). DOI: https://doi.org/10.1016/j.powtec.2009.05.001

[8] A. Yu, J. Hall, Packing of Fine Powders Subjected to Tapping. Powder Technol. **78** (3), 247-256 (1994). DOI: https://doi.org/10.1016/0032-5910(93)02790-H

[9] E.O. Olakanmi, Effect of Mixing Time on the Bed Density, and Microstructure of Selective Laser Sintered (SLS) Aluminium Powders. Mater. Res. **15** (2) 167-176 (2012). DOI: https://doi.org/10.1590/S1516-14392012005000031

[10] P.W. Cleary, M.L. Sawley, DEM Modelling of Industrial Granular Flows: 3D Case Studies and the Effect of Particle Shape on Hopper Discharge. Appl. Math. Model. **26**(2), 89-111(2002). DOI: https://doi.org/10.1016/S0307-904X(01)00050-6

[11] R.M. German, Prediction of Sintered Density for Bimodal Powder Mixtures. Metall. Mater. Trans. A. **23**, 1455-1465 (1992). DOI: https://doi.org/10.1007/BF02647329

[12] L. Cordova, M. Campos, T. Tinga, Revealing the Effects of Powder Reuse for Selective Laser Melting by Powder Characterization. JOM-US. **71**, 1062-1072 (2019). DOI: https://doi.org/10.1007/s11837-018-3305-2

[13] Y. Liu, X. Guo, H. Lu, X. Gong, An Investigation of the Effect of Particle Size on the Flow Behavior of Pulverized Coal. Procedia Eng. **102**, 698-713 (2015). DOI: https://doi.org/10.1016/j.proeng.2015.01.170

[14] I. Tomasetta, D. Barletta, M. Poletto, The Effect of Temperature on Flow Properties of Fine Powders. Chem. Eng. Trans. **24**, 655-660(2011). DOI: https://doi.org/10.3303/CET1124110

[15] C. Schadauer, G.R. Martetschläger, A.L. Ilie, A. Angerbauer, C. Lanzerstorfer, Casting Powders: Influence of the Humidity on the Flowability. Ironmak. Steelmak. **47**, 460-463 (2020). DOI: https://doi.org/10.1080/03019233.2020.1725730

[16] L. Marchetti, P. Mellin, C. Neil Hulme, Negative Impact of Humidity on the Flowability of Steel Powders. Part. Sci. Technol. **40**, 722-736 (2022). DOI: https://doi.org/10.1080/02726351.2021.1995091

[17] J. Hu, C. Liang, C.-Y. Wu, X. Wang, Q. Zhou, Effect of Electrostatic Interactions on Particle Dispersion in a Rotating Spherical Container. Powder Technol. **398**, 117063 (2022). DOI: https://doi.org/10.1016/j.powtec.2021.117063

[18] Y. Ma, T.M. Evans, N. Philips, N. Cunningham, Numerical Simulation of the Effect of Fine Fraction on the Flowability of Powders in Additive Manufacturing. Powder Technol. **360**, 608-621 (2020). DOI: https://doi.org/10.1016/j.powtec.2019.10.041

[19] I. Yadroitsev, A. Gusarov, I. Yadroitsava, I. Smurov, Single Track Formation in Selective Laser Melting of Metal Powders. J. Mater. Process. Technol. **210** (19), 1624-1631 (2010). DOI: https://doi.org/10.1016/j.jmatprotec.2010.05.010

[20] N. Zeoli, S. Gu, Numerical Modelling of Droplet Break-up for Gas Atomisation. Comput. Mater. Sci. **38** (2), 282-292 (2006). DOI: https://doi.org/10.1016/j.commatsci.2006.02.012

[21] J. Xie, Y. Zhao, J. Dunkley, Effects of Processing Conditions on Powder Particle Size and Morphology in Centrifugal Atomisation of Tin. Powder Metall. **47**, 168-172 (2004). DOI: https://doi.org/10.1179/003258904225015482

[22] D. Schwenck, N. Ellendt, J. Fischer-Bühner, P. Hofmann, V. Uhlenwinkel, A Novel Convergent–Divergent Annular Noz-

zle Design for Close-Coupled Atomisation. Powder Metall. **60**, 198-207 (2017).
DOI: https://doi.org/10.1080/00325899.2017.1291098

[23] A. Allimant, M. Planche, Y. Bailly, L. Dembinski, C. Coddet, Progress in Gas Atomization of Liquid Metals by Means of a De Laval Nozzle. Powder Technol. **190**, 79-83 (2009).
DOI: https://doi.org/10.1016/j.powtec.2008.04.071

[24] W.S. Prashanth, S.L. Thotarath, S. Sarkar, T.N.C. Anand, S. Bakshi, Experimental Investigation on the Effect of Melt Delivery Tube Position on Liquid Metal Atomization. Adv. Powder Technol. **32** (3), 693-701 (2021).
DOI: https://doi.org/10.1016/j.apt.2021.01.017

[25] J. Wang, M. Xia, J. Wu, C. Ge, Ladle Nozzle Clogging in Vacuum Induction Melting Gas Atomization: Influence of the Melt Viscosity. Metall. and Mater. Trans. B. **53**, 2386-2397 (2022).
DOI: https://doi.org/10.1007/s11663-022-02537-y

[26] L.J. Jallo, M. Schoenitz, E.L. Dreizin, R.N. Dave, C.E. Johnson, The Effect of Surface Modification of Aluminum Powder on Its Flowability, Combustion and Reactivity. Powder Technol. **204** (1), 63-70 (2010).
DOI: https://doi.org/10.1016/j.powtec.2010.07.017

[27] M. Ramlakhan, C.Y. Wu, S. Watano, R.N. Dave, R. Pfeffer, Dry Particle Coating Using Magnetically Assisted Impaction Coating: Modification of Surface Properties and Optimization of System and Operating Parameters. Powder Technol. **112**, 137-148 (2000).
DOI: https://doi.org/10.1016/S0032-5910(99)00314-9

[28] S. Kumar, S.R. Kumar, S.C. Vettivel, Tribological Behavior of Sintered Electrolytic Iron-zinc Stearate Added Compacts. Materialwissenschaft und Werkstofftechnik **54** (5), 627-636 (2023).
DOI: https://doi.org/10.1002/mawe.202200251

[29] Z. Liu, H. Li, X. Liu, Effect of Warm Compaction Lubricant on the Properties of Fe-based Powder Metallurgy Materials. Mater. Res. Express **6** (4), 046534 (2019).
DOI: https://doi.org/10.1088/2053-1591/aafbfa

[30] L.C. Zhang, W.Y. Xu, Z. Li, L. Zheng, Y.F. Liu, G.Q. Zhang, Characterization of Particle Shape of Nickel-Based Superalloy Powders Using Image Processing Techniques. Powder Technol. **395**, 787-801 (2022).
DOI: https://doi.org/10.1016/j.powtec.2021.10.013

[31] H. Rumpf, Zur Theorie der Zugfestigkeit von Agglomeraten bei Kraftübertragung an Kontaktpunkten. Chem. Ing. Tech. **42**, 538-540 (1970). DOI: https://doi.org/10.1002/cite.330420806

[32] K. Yuasa, M. Tagami, M. Yonehara, T.T. Ikeshoji, K. Takeshita, H. Aoki, H. Kyogoku, Influences of Powder Characteristics and Recoating Conditions on Surface Morphology of Powder Bed in Metal Additive Manufacturing. Int. J. Adv. Manuf. Technol. **115**, 3919-3932 (2021).
DOI: https://doi.org/10.1007/s00170-021-07359-x

[33] G. Marchese, G. Basile, E. Bassini, Study of the Microstructure and Cracking Mechanisms of Hastelloy X Produced by Laser Powder Bed Fusion. Materials **11** (1), 106 (2018).
DOI: https://doi.org/10.3390/ma11010106

[34] H.C. Hamaker, The London-van Der Waals Attraction between Spherical Particles. Physica **4** (10), 1058-1072 (1937).
DOI: https://doi.org/10.1016/S0031-8914(37)80203-7

[35] H. Shi, R. Mohanty, S. Chakravarty, R. Cabiscol, M. Morgeneyer, H. Zetzener, J.Y. Ooi, A. Kwade, S. Luding, V. Magnanimo, Effect of Particle Size and Cohesion on Powder Yielding and Flow. Kona Powder Part. J. **35**, 226-250 (2018).
DOI: https://doi.org/10.14356/kona.2018014

[36] C. Machio, R. Machaka, H. Chikwanda, Consolidation of Titanium Hydride Powders during the Production of Titanium PM Parts: The Effect of Die Wall Lubricants. Mater. Des. **90**, 757-766 (2016).
DOI: https://doi.org/10.1016/j.matdes.2015.11.030

[37] L.Y. Leung, C. Mao, I. Srivastava, P. Du, C.Y. Yang, Flow Function of Pharmaceutical Powders is Predominantly Governed by Cohesion, not by Friction Coefficients. J. Pharm. Sci. **106**, 1865-1873 (2017). DOI: https://doi.org/10.1016/j.xphs.2017.04.012

[38] W. Qi, B. Huang, M. Wang, Z. Li, Z. Yu, Generalized Bond-Energy Model for Cohesive Energy of Small Metallic Particles. Phys. Lett. A. **370**, 494-498 (2007).
DOI: https://doi.org/10.1016/j.physleta.2007.06.062

[39] Q. Li, B. Zhang, Y. Wen, et al., A comprehensive study of tantalum powder preparation for additive manufacturing. Applied Surface Science **593**, 153357 (2022).
DOI: https://doi.org/10.1016/j.apsusc.2022.153357

[40] C. Liu, K. Zhu, W. Ding, Y. Liu, G. Chen, X. Qu, Additive Manufacturing of WMoTaTi Refractory High-Entropy Alloy by Employing Fluidised Powders, Powder Metall. **65** (5), 413-425 (2022). DOI: https://doi.org/10.1080/00325899.2022.2031718

[41] G. Gai, Y. Yang, L. Jin, X. Zou, Y. Wu, Particle Shape Modification and Related Property Improvements. Powder Technol. **183** (1), 115-121(2008).
DOI: https://doi.org/10.1016/j.powtec.2007.11.026

[42] T. Marcu, M. Todea, I. Gligor, P. Berce, C. Popa, Effect of Surface Conditioning on the Flowability of Ti6Al7Nb Powder for Selective Laser Melting Applications. Appl. Surf. Sci. **258** (7), 3276-3282 (2012). DOI: https://doi.org/10.1016/j.apsusc.2011.11.081

[43] W. Ding, Z. Wang, G. Chen, W. Cai, C. Zhang, Q. Tao, X. Qu, M. Qin, Oxidation Behavior of Low-Cost CP-Ti Powders for Additive Manufacturing via Fluidization. Corros. Sci. **178**, 109080 (2021). DOI: https://doi.org/10.1016/j.corsci.2020.109080